




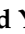


## Article

# Synthesis of Bivalent Ni(II), Cu(II) and Zn(II) Complexes of Azodicarbonamide in Mixture of Methanol and Aqueous Solvents: Spectral Characterizations and Anti-Microbial Studies

Ayman A. O. Younes<sup>1</sup>, Abdel Majid A. Adam<sup>2</sup>, Moamen S. Refat<sup>2,\*</sup>, Asma S. Al-Wasidi<sup>3</sup>,  
Abdulrahman A. Almehezia<sup>4</sup>, Mohamed A. Al-Omar<sup>4</sup>, Ahmed M. Naglah<sup>4,\*</sup>, Abdulrahman M. Al-Obaid<sup>5</sup>,  
Hamad M. Alkahtani<sup>5</sup>, Ahmad J. Obaidullah<sup>5</sup>, Mohamed Y. El-Sayed<sup>6</sup> and Kareem A. Asla<sup>7</sup>

<sup>1</sup> Department of Chemistry, Faculty of Science, University of Bisha, Bisha 61922, Saudi Arabia

<sup>2</sup> Department of Chemistry, College of Science, Taif University, P.O. Box 11099, Taif 21944, Saudi Arabia

<sup>3</sup> Department of Chemistry, College of Science, Princess Nourah Bint Abdulrahman University, Riyadh 11671, Saudi Arabia

<sup>4</sup> Drug Exploration and Development Chair (DEDC), Department of Pharmaceutical Chemistry, College of Pharmacy, King Saud University, Riyadh 11451, Saudi Arabia

<sup>5</sup> Department of Pharmaceutical Chemistry, College of Pharmacy, King Saud University, Riyadh 11451, Saudi Arabia

<sup>6</sup> Chemistry Department, College of Science, Jouf University, Sakaka 2014, Saudi Arabia

<sup>7</sup> Department of Chemistry, Faculty of Science, Zagazig University, Zagazig, 44519, Egypt

\* Correspondence: moamen@tu.edu.sa (M.S.R.); anaglah@ksu.edu.sa (A.M.N.)

**Abstract:** Three new transition-metal complexes were produced by refluxing azodicarbonamide (ADCA) with nickel(II), copper(II), and zinc(II) solutions in a mixture of 50% (*v/v*) methanol and water. The magnitude of chelation between metal ions and ligand molecules was assessed by FT-IR, UV, elemental analysis, TGA, conductivity, mass, and magnetic susceptibility measurements. FT-IR analysis suggested a bi-dentate chelation in all complexes, which takes place through the N-azo and O-carbonyl groups. Based on the measurement of magnetic moments and spectral analysis, a distorted octahedral geometry was proposed for Ni(II) and Cu(II) complexes, whereas zinc complex showed a hexa-coordinated geometry. The optical band gaps of the nickel(II), copper(II) and zinc(II) complexes were found to be 1.91, 2.50, and 1.96 eV, respectively, which means that they can be employed as semiconductors and that they are in the same range as highly effective photovoltaic materials. The Urbach energy parameters were also estimated from other optical parameters. The biological activity of azodicarbonamide and its synthesized complexes has been screened against the selected gram bacteria (+ve) and fungi.

**Keywords:** azodicarbonamide; transition metal complexes; bioactivity; thermal analysis; optical properties



**Citation:** Younes, A.A.O.; Adam, A.M.A.; Refat, M.S.; Al-Wasidi, A.S.; Almehezia, A.A.; Al-Omar, M.A.; Naglah, A.M.; Al-Obaid, A.M.; Alkahtani, H.M.; Obaidullah, A.J.; et al. Synthesis of Bivalent Ni(II), Cu(II) and Zn(II) Complexes of Azodicarbonamide in Mixture of Methanol and Aqueous Solvents: Spectral Characterizations and Anti-Microbial Studies. *Crystals* **2023**, *13*, 367. <https://doi.org/10.3390/cryst13030367>

Academic Editor: Marian Valko

Received: 23 January 2023

Revised: 14 February 2023

Accepted: 15 February 2023

Published: 21 February 2023



**Copyright:** © 2023 by the authors. Licensee MDPI, Basel, Switzerland. This article is an open access article distributed under the terms and conditions of the Creative Commons Attribution (CC BY) license (<https://creativecommons.org/licenses/by/4.0/>).

## 1. Introduction

Azodicarbonamide (ADCA; Figure 1) is a yellow powder that is frequently employed in industry as a foaming agent [1–3] in the creation of numerous products; it is non-toxic, odorless, and non-polluting when decomposed. Among the gases produced by the decomposition of ADCA are 65% N<sub>2</sub> gas, 24% CO, 5% CO<sub>2</sub>, and 5% ammonia [4–6]. The structure of azodicarbonamide is as follows [7]:

The current procedure for the decomposition of ADCA is as follows: Hydrazodicarbonamide (biurea) is synthesized from hydrazine hydrate and urea by means of an acid condensation reaction [8], and ADCA is produced via an oxidation process from biurea. By oxidizing biurea, there are various ways to make azodicarbonamide, and these include the chlorate method, the chlorine method, the hydrogen peroxide method, and the dichromate oxidizing agent framework [8,9]. Due to its advantages, including its improvement of gluten products and its low cost, azodicarbonamide is employed as a dough conditioner [10–12]. Generally, azodicarbonamide will not interact with flour directly, but

when wheat is mixed with water to form dough, it may produce reactive oxygen. The sulfhydryl group (-sh) of protein amino acids in wheat will be oxidized by the reactive oxygen forming disulfide bonds (-s-s), which will connect the protein chains to one another to form a mesh structure. It is well known that the addition of initiators, specifically the salts of zinc and calcium, can lower the temperature at which azodicarbonamide decomposes, according to several researchers [13,14], when azodicarbonamide interacts with calcium- or zinc-based salts, the resulting salts of azodicarboxylic acid serving as the catalyst for temperature breakdown. Additionally, the Lewis acid-base reaction, in which the metal of the activating addition functions as a Lewis acid by accepting electrons, is the activation mechanism of the azodicarbonamide decomposition process, and azodicarbonamide acts as the base—that is, it is an electron pair donor. The possibility that metals possessing filled pre-outer d-electron orbitals could form complexes with azodicarbonamide molecules as ligands was also assumed [15]. A break in the -c-n= bond is made easier by the synthesis of complexes, which results in a lack of electron density around the n-c bond of the azo-group.

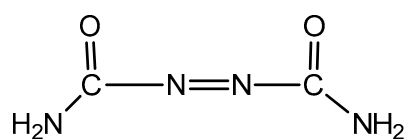


Figure 1. The molecular formula of ADCA.

## 2. Materials and Methods

### 2.1. Equipment's

Azodicarbonamide and its metal complexes were characterized using different techniques. CNH elemental analysis was replicated three times using a LECO analyzer (Micro TruSpec model) to ensure the reproducibility of the results. On a Perkin-Elmer 1000 FTIR spectrophotometer, the FT-IR spectra of the complexes were measured using KBr-disc. The measurement of UV-Visible spectra for compounds was carried out in DMF solutions on a UNICAM UV-300 spectrophotometer (thickness of cuvette, 1 cm). Using a TGA Perkin Elmer thermal analyzer, a thermal analysis (TG and DTG) was carried out at 25–950 °C with the heating rate 10 °C min<sup>-1</sup>. The measurement of magnetic susceptibilities was carried out at 25 °C using Balance, Sherwood Scientific, Cambridge Science Park Cambridge, England.

### 2.2. Synthesis of Azodicarbonamide Systems

All the chemicals utilized in this study were ultra-fine and did not require additional purification. Azodicarbonamide purchased from (Fluka Chemical Co. 99.9%), Cu(NO<sub>3</sub>)<sub>2</sub>·6H<sub>2</sub>O, ZnCl<sub>2</sub> and NiCl<sub>2</sub>·xH<sub>2</sub>O (99.9%, Aldrich Chemical Co., USA). NiCl<sub>2</sub>·6H<sub>2</sub>O, Cu(NO<sub>3</sub>)<sub>2</sub>·6H<sub>2</sub>O, and ZnCl<sub>2</sub> (1 mmol) were added to azodicarbonamide (2 mmol) in a mixture of 50% (v/v) methanol and water to create 40 mL of three azodicarbonamide systems. Colored precipitates were produced by refluxing the reaction mixtures for about 3–5 h at suitable temperatures. The precipitates were filtered-off and washed with MeOH and water, after which it was dried under CaCl<sub>2</sub> in a desiccator. About 73–79% of the yields were produced.

### 2.3. Anti-Microbial Assay

The diffusion method [16,17] was utilized to determine the inhibition zone of azodicarbonamide and its complexes against G (+ve) bacteria (*Bacillus subtilis* and *Aspergillus oryzae*) and fungi (*Penicillium* sp.). Dimethyl sulfoxide was used as the control solvent. Two different concentrations, 3 mg/mL and 6 mg/mL, were used in agar plates that were incubated at 37 ± 0.5 °C for 24 h.

### 3. Result and Discussion

#### 3.1. Elemental and Conductance Data and Magnetic Moment

A new series of azodicarbonamide complexes have been produced from refluxing azodicarbonamide with alcoholic Ni(II), Cu(II), and Zn(II) solutions. The obtained compounds are air-stable and soluble in dimethylsulphoxide and dimethylformamide organic solvents. The molar conductance measurements of ADCA and its complexes were carried out in a DMSO solution and revealed the non-electrolytic nature as well as the neutral form of the prepared compounds. The stoichiometry of the compounds was confirmed by the elemental analysis results, which closely matched the calculated values. The electronic spectra as well as the characteristic infrared bands were taken into consideration as additional evidence of the suggested geometry of compounds. The microanalytical investigation information of the complexes found a 1:2 stoichiometry (metal: ligand) with molecular formulae  $[\text{Ni}(\text{ADCA})_2(\text{Cl})_2] \cdot 1.5\text{H}_2\text{O}$  (1),  $[\text{Cu}(\text{ADCA})_2(\text{NO}_3)_2] \cdot \text{H}_2\text{O}$  (2), and  $[\text{Zn}(\text{ADCA})_2(\text{Cl})_2] \cdot \text{H}_2\text{O}$  (3), where ADCA is  $\text{C}_2\text{H}_4\text{N}_4\text{O}_2$  (Figure 2). The physical data: the conductance, magnetic, and elemental analysis results are listed in Table 1.

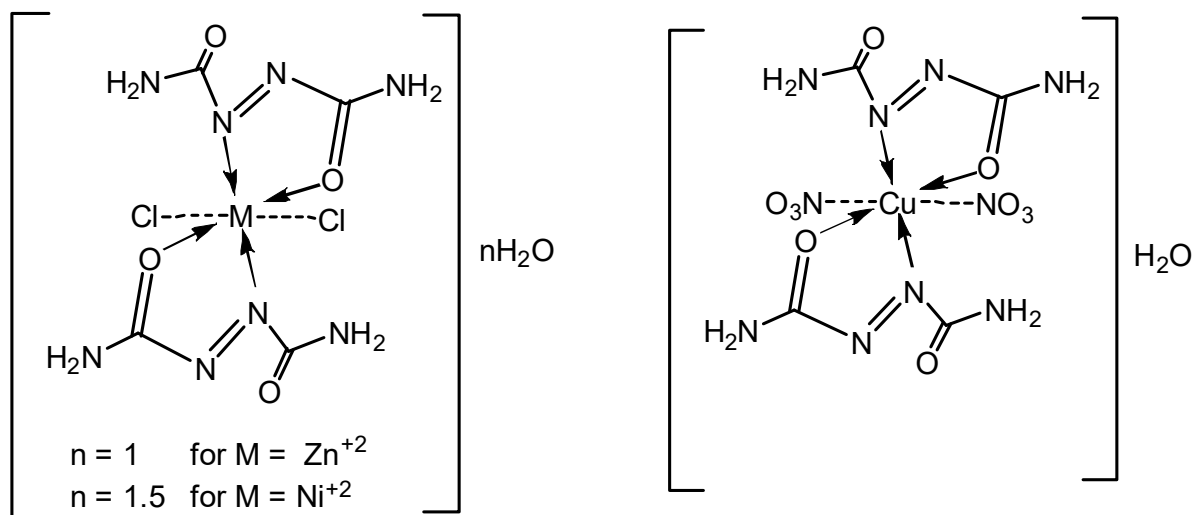


Figure 2. The proposed structures of the synthesized complexes.

Table 1. Micro analytical and physical data for azodicarbonamide and its complexes.

Compounds	Yield%	Mp/°C	Color	Conductance ( $\text{ohm}^{-1} \cdot \text{cm}^2 \cdot \text{mol}^{-1}$ )	$\mu_{\text{eff}}$ (B.M)	Element	Found	Calc.
$\text{NH}_2\text{CON}=\text{NCONH}_2$	-	245	White	11	-	%C	20.69	20.69
						%H	3.47	3.45
						%N	48.57	48.27
$[\text{Ni}(\text{ADCA})_2(\text{Cl})_2] \cdot 1.5\text{H}_2\text{O}$	79	>350	Light green	10	3.46	%C	12.52	12.34
						%H	2.86	2.83
						%N	28.38	28.79
$[\text{Cu}(\text{ADCA})_2(\text{NO}_3)_2] \cdot \text{H}_2\text{O}$	75	>350	Dark green	7	1.93	%C	10.97	10.96
						%H	2.21	2.28
						%N	31.71	31.96
$[\text{Zn}(\text{ADCA})_2(\text{Cl})_2] \cdot \text{H}_2\text{O}$	73	>350	Yellow	13	Dia	%C	13.05	12.43
						%H	2.60	2.59
						%N	28.36	29.02

#### 3.2. Magnetic Properties

All the complexes under consideration were found to be paramagnetic on the basis of the magnetic moment measurements taken from Table 1, with the exception of the

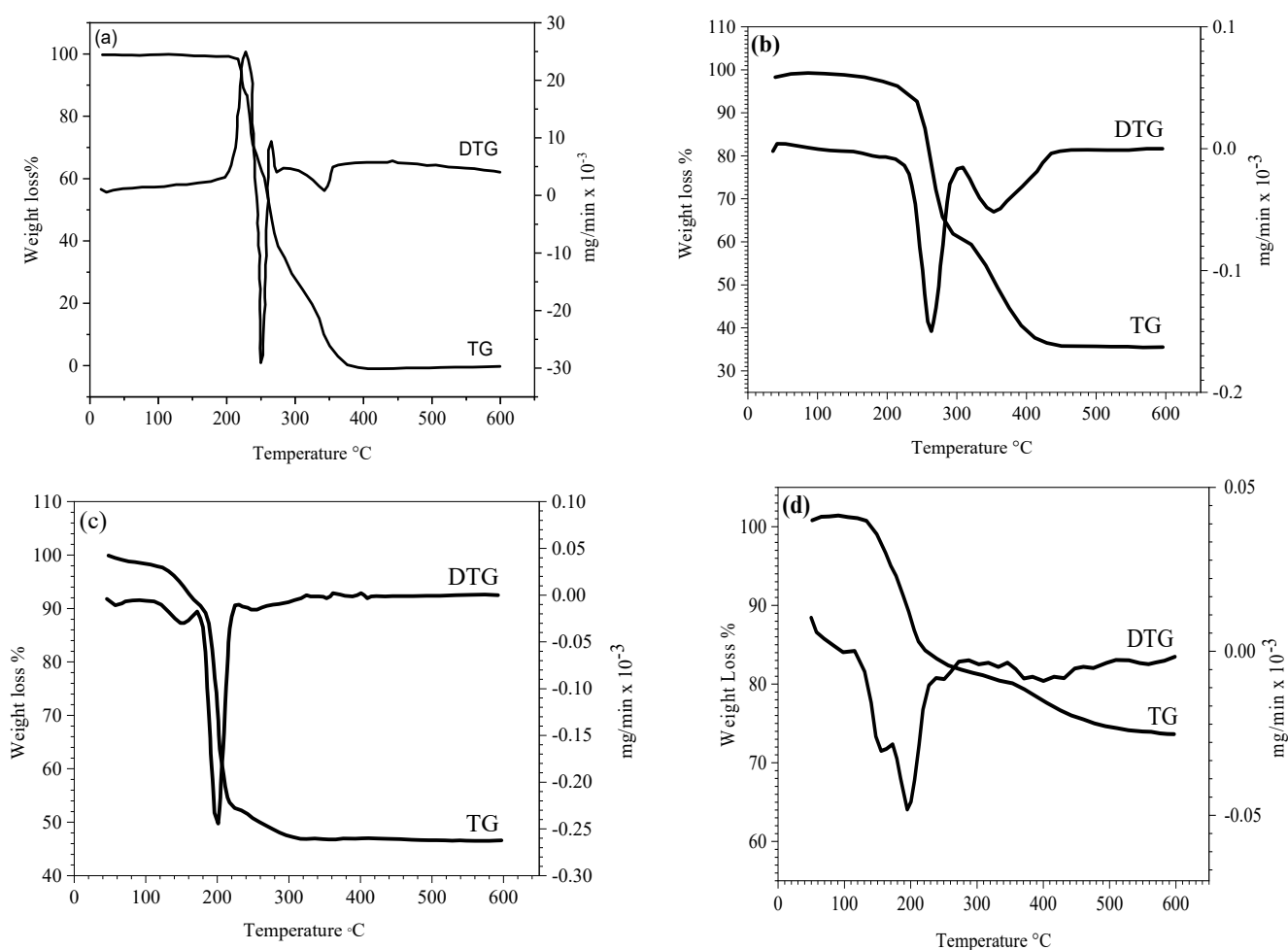
diamagnetic zinc(II) complex, which exhibited a hexa-coordinated geometry because of the measuring temperature affecting the precise value of the magnetic moment and the spin-orbit coupling's magnitude. All observations were made at ambient temperature. At room temperature, the magnetic moment of the solid nickel (II) complex was found to be 3.46 B.M, which lies within the range of experimental data (3.32 B.M) and is indicative of two unpaired electrons per Ni(II) ion in an octahedral environment. The Cu(II) complex showed an  $\mu_{\text{eff}}$  value of 1.93 B.M, which is in agreement with the experimental range (1.96 B.M) and is indicative of one unpaired electron per Cu(II) ion, suggesting these complexes within the range are consistent with spin-free distorted octahedral geometry.

### 3.3. IR Spectra of Azodicarbonamide and Its Complexes

The comparison of the IR spectra of the complexes with those of azodicarbonamide determine the kind and site of coordination that may be involved in chelation. The most important experimental and theoretically calculated IR spectral main bands of azodicarbonamide and of its metal complexes are given in Table 2 and shown in Figure S1a–d with their tentative assignments. The bands at  $1727\text{ cm}^{-1}$  in the IR spectrum are assigned to a superposition of the stretching vibrations of C=O and N-C, which are more strongly infrared-active. The bands of azodicarbonamide observed at  $1116\text{ cm}^{-1}$  in the IR spectrum are assigned to the same vibration, namely a superposition of the deformation bands of  $\text{NH}_2$  and the stretching vibrations of C=O and N-C. The bands at  $1330\text{ cm}^{-1}$  in the IR spectrum and at  $1332\text{ cm}^{-1}$  are assigned to a superposition of the deformation bands of  $\text{NH}_2$ , the N-C stretching vibration, and the N-C=O bending vibration. The strong characteristic band can be observed in the IR spectrum of azodicarbonamide (Figure 3a) located at  $1728\text{ cm}^{-1}$ , which is assigned to the stretching vibration of C=O [18]. Azodicarbonamide has two probable sites for the coordination to metals containing azo and C=O groups [19]. The observed wavenumber shifts and the broadening in the azodicarbonamide spectrum were considered the result of intermolecular hydrogen bonding interactions [20]. However, these intermolecular hydrogen bonds break upon coordination to metals. The strong carbonyl stretching peak at  $1728\text{ cm}^{-1}$  in azodicarbonamide shifts to  $1621$ ,  $1556$ , and  $1679\text{ cm}^{-1}$ , which indicates the interaction of the carbonyl and copper (II) ion and the Zinc (II) and nickel (II) ion within the coordination compound. The coordination of the azodicarbonamide with the metal ions was further confirmed by the appearance of new bands between  $551\text{--}585$  and  $407\text{--}465\text{ cm}^{-1}$ , which were designated to the metal nitrogen (M-N) and metal-oxygen (M-O) extending vibrations individually. These bands were not present in the spectra of the free ligand, thus affirming the participation of O and N in the coordination with transition metal ions [21,22]. Therefore, the IR spectra shows that the ligand azodicarbonamide is bidentate and coordinates to the metal through the nitrogen atom of the azo group and the oxygen atom of carbonyl groups [19].

**Table 2.** Vibrational assignment of important IR bands of the azodicarbonamide ligand and its metal complexes.

Assignments	Compounds			
	$\text{NH}_2\text{CON}=\text{NCONH}_2$	$[\text{Cu}(\text{ADCA})_2(\text{NO}_3)_2]\cdot\text{H}_2\text{O}$	$[\text{Zn}(\text{ADCA})_2(\text{Cl})_2]\cdot\text{H}_2\text{O}$	$[\text{Ni}(\text{ADCA})_2(\text{Cl})_2]\cdot 1.5\text{H}_2\text{O}$
$\delta\text{N-C=O} + \delta\text{NCN} + \delta\text{C-N=N}$	636	608	563	620
$\delta\text{C=O} + \delta\text{H-N-H} + \delta\text{N}=\text{N}$	752	777.2	713	764
$\delta\text{N-H}$	856	840	831	997
$\delta\text{H-N-H} + \nu\text{C-N} + \delta\text{N-C=O}$	1116	1043	1042	1110
$\delta\text{H-N-H} + \nu\text{C-N} + \delta\text{N-C=O}$	1330	1344	1387	1419
$\nu\text{C=O} + \nu\text{C-N}$	1727	1621	1556	1679
$\nu(\text{M-O})$	-	438	465	407
$\nu(\text{M-N})$	-	585	572	551



**Figure 3.** TG and DTG thermograms of (a) azodicarbonamide (b) Ni(II), (c) Cu(II), and (d) Zn(II) complexes.

### 3.4. Thermal Studies

Thermogravimetric analysis is used to investigate azodicarbonamide and its metal complexes at 25–1000 °C in a nitrogen environment (Table 3 & Figure 3). The DTG curves show the rate of weight loss versus the temperature scale, while the TGA curves show the percentage mass loss as a function of the temperature. When azodicarbonamide breaks down between 165 and 195 °C, gas is released along with the formation of a residue. The gas is made up of N<sub>2</sub>, CO gases, and a third substance that, depending on the temperature, is either ammonia or HNCO acid. The residue is a combination of biurea, HNCO, and H<sub>3</sub>N<sub>3</sub>C<sub>2</sub>O<sub>2</sub>, whereas the sublimate is made up of HNCO, cyamelide, and urea [23–27]. Two major reactions, (i) and (ii), seem to occur simultaneously in the first mode of decomposition, in which azodicarbonamide breaks down to create biurea. HNCO and N<sub>2</sub> in the second mode of decomposition breakdown to create ammonia, N<sub>2</sub>, HNCO, and H<sub>3</sub>N<sub>3</sub>C<sub>2</sub>O<sub>2</sub>. The first mode of decomposition occurs twice as frequently as the second at 171.5 °C, while it appears that isocyanic acid's secondary reactions produce cyanuric acid, cyamelide, carbon monoxide, and urea. The biurea that was initially created breaks down into urazole and ammonia at higher temperatures [27,28]. The sequence for the thermal degradation of azodicarbonamide is given (Scheme S1).

The [Ni(C<sub>2</sub>H<sub>4</sub>N<sub>4</sub>O<sub>2</sub>)<sub>2</sub>(Cl)<sub>2</sub>].1.5H<sub>2</sub>O thermogram reveals three main decomposition steps. In the first step, T<sub>max</sub> = 265 °C, and the residue is 0.5HCNO + 2Cl<sup>-</sup> + N<sub>2</sub> + 1.5H<sub>2</sub>O with a weight loss percent of 39.12 (calc 38.95%). In the second step, T<sub>max</sub> = 353.51 °C, and the residue is C<sub>2</sub>N<sub>2</sub>O<sub>2</sub> + 0.5HCN with a weight loss percent of 25.75 (calc 25.66%). In the final step, the final residue is 1.5NH<sub>3</sub> + 0.5HCN + N<sub>2</sub> + NiO with a weight loss

of 36.13% (calc 35.05%). The  $[\text{Cu}(\text{C}_2\text{H}_4\text{N}_4\text{O}_2)_2(\text{NO}_3)_2]\cdot\text{H}_2\text{O}$  thermogram reveals three degradation steps within the temperature range 45–1000 °C. In the first step,  $T_{\text{max}} = 45$  °C with a weight loss of 8.981% (calc 9.541%), corresponding to the loss of  $\text{H}_2\text{O} + \text{HNCO}$ . In the second step,  $T_{\text{max}} = 250$  °C and is accompanied by a weight loss of 41.065% (calc 41.675%), corresponding to the loss of  $\text{HNCO} + \text{C}_2\text{H}_3\text{N}_3\text{O}_2 + \text{N}_2 + 0.5\text{NH}_3$ . Then, the final thermal decomposition product obtained is  $0.5\text{NH}_3 + 2\text{NO}_3 + \text{CuO} + 0.5\text{C}$ . In the  $[\text{Zn}(\text{C}_2\text{H}_4\text{N}_4\text{O}_2)_2(\text{Cl})_2]\cdot\text{H}_2\text{O}$  thermogram, decomposition occurs in four steps. In the first step,  $T_{\text{max}} = 158$  °C, with a weight loss of 8.371% (calc. 8.02%), corresponding to the loss of  $\text{H}_2\text{O} + \text{N}_2$ . In the second step,  $T_{\text{max}} = 197$  °C, corresponding to the losses of  $\text{NH}_3 + \text{HCN}$  with weight losses of 14.034% (calc. 15.55%). In the third step,  $T_{\text{max}} = 538$  °C, corresponding to the loss of  $\text{Cl}^- + \text{HCN}$  with a weight loss of 28.19% (calc 25.13%). Finally,  $\text{C}_2\text{H}_3\text{N}_3\text{O}_2 + \text{ZnO} + 2\text{C}$  is obtained through the final decomposition step.

**Table 3.** The maximum temperature,  $T_{\text{max}}$  (°C), and weight loss values of the decomposition stages for azodicarbonamide metal complexes.

Compounds	TGA Range (°C)	Number of Peaks	Weight Loss (%)		Lost Species
			Calc.	Found	
$[\text{Ni}(\text{ADCA})_2(\text{Cl})_2]\cdot 1.5\text{H}_2\text{O}$ $M_w = 379.95$	0–265	1	38.12	38.66	$0.5\text{HCNO} + 1.5\text{H}_2\text{O} + \text{N}_2 + 2\text{Cl}$
	265–353	1	25.75	25.66	$\text{C}_2\text{N}_2\text{O}_2 + 0.5\text{HCN}$
	353–800	Residue	36.13	35.761	$1.5\text{NH}_3 + 0.5\text{HCN} + 0.5\text{HCNO} + \text{NiO}\downarrow$
$[\text{Cu}(\text{ADCA})_2(\text{NO}_3)_2]\cdot\text{H}_2\text{O}$ $M_w = 439.74$	10–139	1	9.514	8.981	$\text{H}_2\text{O} + \text{HNCO}$
	135–250	1	41.675	41.065	$\text{HNCO} + \text{C}_2\text{H}_3\text{N}_3\text{O}_2 + \text{N}_2 + 0.5\text{NH}_3$
	250–600	Residue	48.811	48.095	$0.5\text{NH}_3 + 2\text{NO}_3 + \text{CuO}\downarrow + 0.5\text{C}\downarrow$
$[\text{Zn}(\text{ADCA})_2(\text{Cl})_2]\cdot\text{H}_2\text{O}$ $M_w = 383.94$	0–265	1	8.37	8.02	$\text{H}_2\text{O} + \text{N}_2$
	265–353	1	14.03	15.55	$\text{NH}_3 + \text{HNCO}$
	353	1	28.742	25.13	$2\text{Cl} + \text{HCN}$
	Residue	Residue	48.858	51.3	$\text{C}_2\text{H}_3\text{N}_3\text{O}_2 + \text{ZnO}\downarrow + 7.5\text{C}\downarrow$

### 3.5. Electronic Spectral Measurements

The absorption spectra of the azodicarbonamide ligand and its metal complexes in DMF were recorded over the wavelength range of 200 to 800 nm. As seen in Table 4 and Figure 4, ADCA has three strong absorption bands at 241, 331, and 433 nm, which may be attributed to the  $\pi \rightarrow \pi^*$  and  $n \rightarrow \pi^*$  electronic transitions [29]. The electronic spectrum of the Ni(II) complex exhibited three absorption bands at 717, 564, and 520 nm, which may be assigned to spin-allowed transitions  ${}^3\text{A}_{2g}(\text{F}) \rightarrow {}^3\text{T}_{2g}(\text{F})$ ,  ${}^3\text{A}_{2g}(\text{F}) \rightarrow {}^3\text{T}_{1g}(\text{F})$ , and  ${}^3\text{A}_{2g}(\text{F}) \rightarrow {}^3\text{T}_{2g}(\text{P})$ , as is characteristic of the distorted octahedral geometry of the Ni(II) ion [30,31]. The spectrum of the Cu(II) complex shows two bands in the ultraviolet and visible regions at about 521 and 400 nm, which can be attributed to  ${}^2\text{E}_g \rightarrow {}^2\text{T}_{2g}$  and intra-ligand transitions, respectively [31]. The zinc(II) complex displays an absorption band at 386 nm assignable to the LMCT transition and hexa-coordinated geometry, and this is further supported by its diamagnetic nature and the absence of the d-d band due to its complete  $d^{10}$  electronic configuration.

### 3.6. Optical Band Gap Energy

Tuac's equations [32,33] were used to predict the optical band gap,

$$\alpha h\nu = (h\nu - E_g)^n$$

where  $h\nu$  = the photon energy,  $h$  = Plank constant,  $n = \frac{1}{2}$  and 2 for direct and indirect transitions respectively,  $\alpha$  = the absorption coefficient,  $A$  = an energy-independent constant.

**Table 4.** Absorption data and band assignment of azodicarbonamide ligand and its complexes.

Compound	Electronic Transition, $\lambda_{\text{max}}$ (nm, DMF)	Band Assignments	$E_g$ (eV)	$E_u$ (eV)
$\text{C}_2\text{H}_4\text{N}_4\text{O}_2$	341, 331, 433	$\pi \rightarrow \pi^*$ , $\pi \rightarrow \pi^*$ , $n \rightarrow \pi^*$	3.72	22.94
[Ni(ADCA) $_2$ (Cl) $_2$ ] $\cdot$ 1.5H $_2$ O	717	$^3\text{A}_{2g}(\text{F}) \rightarrow ^3\text{T}_{2g}(\text{F})$	1.91	9.38
	564	$^3\text{A}_{2g}(\text{F}) \rightarrow ^3\text{T}_{1g}(\text{F})$		
	520	$^3\text{A}_{2g}(\text{F}) \rightarrow ^3\text{T}_{2g}(\text{P})$		
[Cu(ADCA) $_2$ (NO $_3$ ) $_2$ ] $\cdot$ H $_2$ O	521	$^2\text{E}_g \rightarrow ^2\text{T}_{2g}$	2.50	4.29
	400	intra-ligand transitions		
[Zn(ADCA) $_2$ (Cl) $_2$ ] $\cdot$ H $_2$ O	236, 327, 386	$\pi \rightarrow \pi^*$ , $n \rightarrow \pi^*$ , L $\rightarrow$ M (LMCT)	1.96	19.83

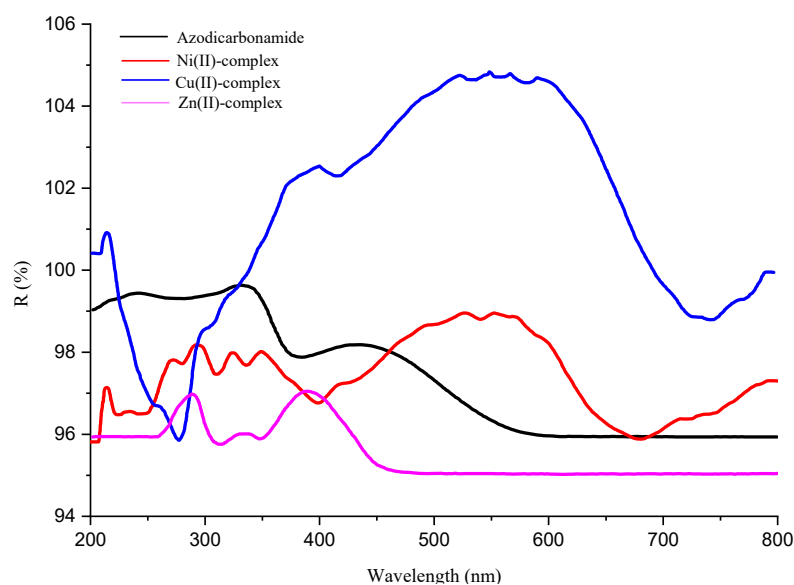
**Figure 4.** UV-Visible spectra of azodicarbonamide and its metal complexes.

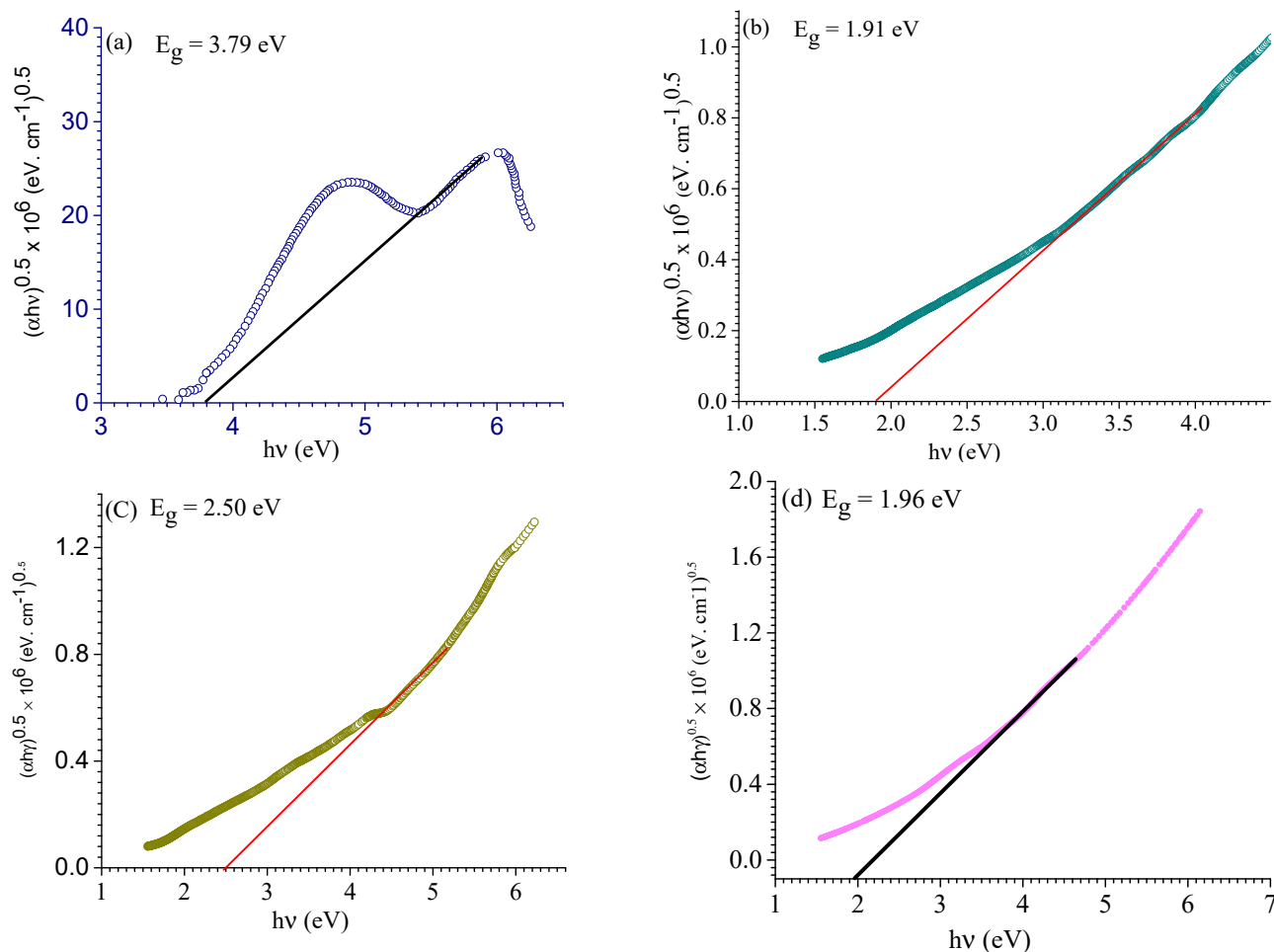
Figure 5 depicts the plotting of  $(\alpha h\nu)^2$  and  $(\alpha h\nu)^{1/2}$  against  $(h\nu)$ . A band gap is obtained by extrapolating the linear component of the curve to  $(\alpha h\nu)^{1/2} = 0$ . The following equation has been used to compute the absorption coefficient ( $\alpha$ ):  $\alpha = 1/d \ln(1/T)$ , where  $d$  = the optical path length of cuvette and  $T$  = estimated transmittance. In the DMF solvent, the band gaps for azodicarbonamide and its Ni(II), Cu(II), and Zn(II) complexes were 3.79, 1.91, 2.50, and 1.96 eV, respectively, and these are listed in Table 4 and Figure 6. To provide insight into the data listed in Table 4, complexation minimizes the  $E_g$  values rather than azodicarbonamide ligand. This decrease in  $E_g$  values is owed to the electron transfer from ligand to metal ion [34]. It is speculated that the presence of Ni or Cu ions in the given complex enhances the mobility of ligand electrons by accepting them in their empty shell. This results in the expansion of the localized levels in the resultant complex, and, as a result, the band gap is narrower and widely utilized in optics, electronics, and energy conversion devices [35]. In fact, a small energy difference facilitates the electron transition between HOMO–LUMO so that the molecule becomes more electro-conductive [36]. The low  $E_g$  values for the studied compounds are in a good agreement with the reported values and, consequently, can be employed as semiconductors as well as highly effective photovoltaic materials [34,37–39].

According to the Urbach formula:

$$\alpha(h\nu) = \alpha_0 \exp(h\nu/E_u)$$

where  $\alpha_0$  = constant,  $E_u$  = the Urbach energy that is interpreted as the width of the localized states.

The absorption coefficient,  $\alpha$ , exponentially depends on the photon energy when  $h\nu \leq E_g$ . From the plot of  $\ln\alpha$  versus  $h\nu$  (Figure 5), the Urbach energy ( $E_u$ ) can be computed and should equal the reciprocal of the slope of the straight line of the linear portion of the curve. The estimated  $E_u$  values are 22.94, 9.377, 4.29, and 19.53 meV, corresponding to azodicarbonamide and its Ni(II), Cu(II), and Zn(II) complexes, respectively. The low  $E_u$  values indicate the minimal defects in the complex structure.



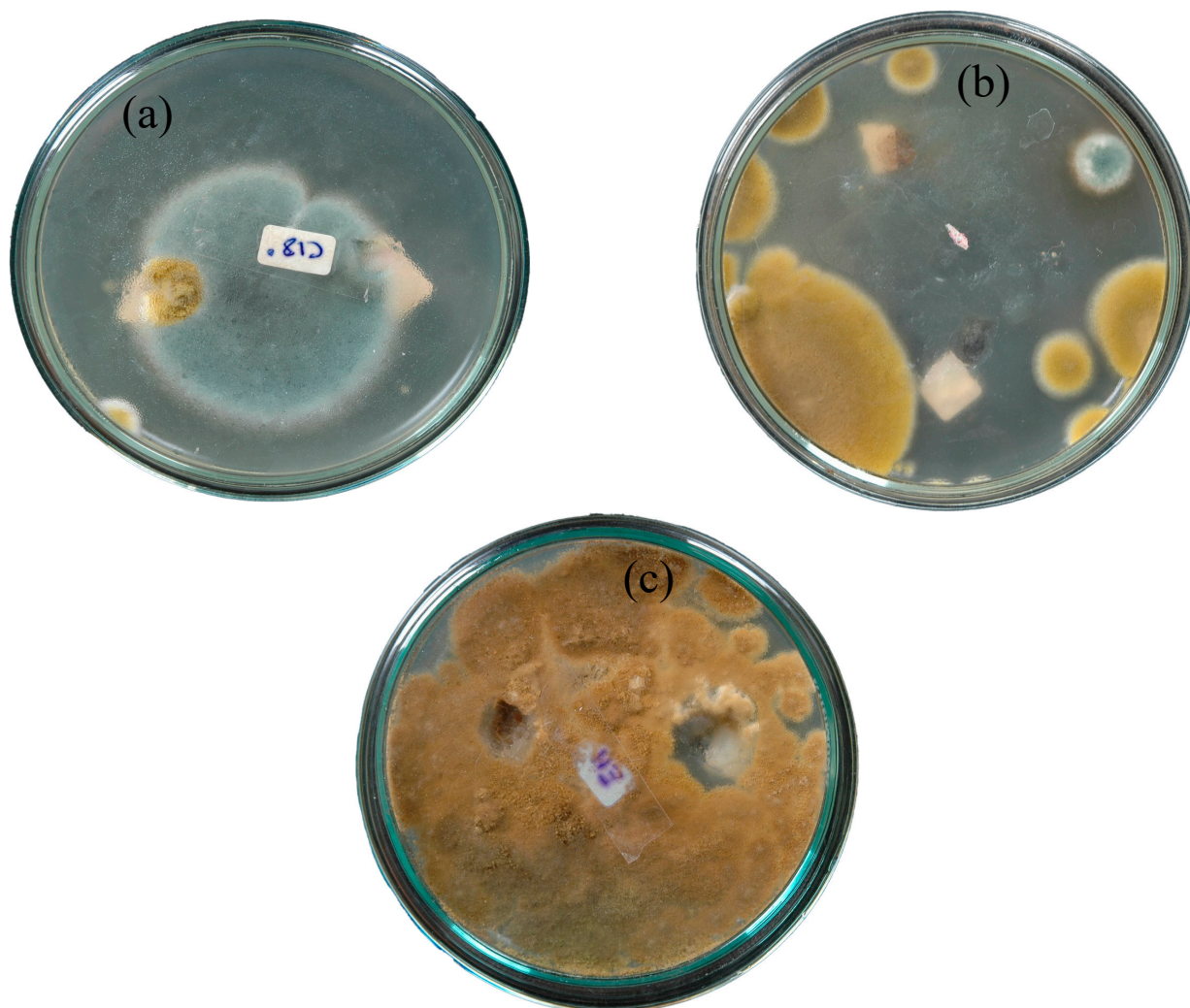
**Figure 5.** Plot of  $(\alpha h\nu)^{0.5}$  vs. photon energy ( $E$ ) of the (a) azodicarbonamide and its (b) Ni(II), (c) Cu(II), and (d) Zn(II) complex.

### 3.7. Mass Spectra of the Azodicarbonamide and Its Metal Complex

The anticipated formulae shown in Figure 2 have been confirmed using the following mass spectral fragmentations of the azodicarbonamide and its Ni(II), Cu(II), and Zn(II) complexes (Figure S2). The mass spectrum of azodicarbonamide having a molecular ion peak at  $m/z = 116.9$  corresponds to  $C_2H_4N_4O_2$ . Meanwhile, another peak at  $m/z = 100.2$  belongs to the  $[C_2H_2N_2O_2]^+$  of the nitroacetonitrile ion. For the structure of guanidine, the hydroxide ion,  $[CH_6N_3O]^+$ , belongs to the peak at  $m/z = 76.1$ . Meanwhile, the last peak at  $m/z = 59.2$  belongs to the diazenylmethanolate ion,  $[CH_3N_2O]^+$ . Additionally, the last peak at  $m/z = 44$  belongs to the aminomethanone ion,  $[CH_2NO]^+$ . Furthermore, the last peak at  $m/z = 30.4$  belongs to the diazenium ion,  $[N_2H_3]^+$  [40] (Scheme S2). The mass spectrum of the Ni(II) complex (Figure S2) shows that the parental ion peak at  $m/z = 279$  belongs to  $[C_4H_5N_7NiO_5]^+$ . The other fragments of the complex give peaks with various intensities at different values such as 243  $[C_4H_3N_5NiO_4]^+$ , 226  $[C_4N_4NiO_4]^+$ , and 164  $[C_2N_2NiO_2]^+$ . The mass spectral fragmentation pattern of Ni(II) complex (Scheme S3) is in agreement with the anticipated structure. The mass spectrum of the Cu(II) complex  $C_4H_{10}CuN_{10}H_{11}$  (Figure S2) shows the molecular ion peak at  $m/z = 375$  corresponding to  $[C_4H_7CuN_9O_9]^+$ . The other fragments of



the complex show the peaks at different values; for example  $[\text{C}_3\text{H}_7\text{CuN}_7\text{O}_3]^+$  has a peak at 251,  $[\text{H}_6\text{CuN}_6\text{O}_2]^+$  has a peak at 211,  $[\text{C}_2\text{H}_3\text{CuN}_5\text{O}_2]^+$  has a peak at 191, and  $[\text{C}_2\text{H}_3\text{N}_5\text{O}]^+$  has a peak at 122. The fragmentation pattern in Scheme S4 is in agreement with the proposed structure of Cu(II) complex. The mass spectra of the Zn(II) complex (Figure S2) show that the molecular ion peaks at  $m/z = 386.6$  belong to the  $[\text{C}_4\text{H}_{10}\text{N}_8\text{O}_5\text{Cl}_2\text{Zn}]^+$ . The other fragments of the complex show that the peaks at  $m/z = 358.46$ ,  $340.46$ ,  $323.46$ ,  $253$ ,  $210.46$ , and  $183.46$  correspond to  $[\text{C}_4\text{H}_{10}\text{Cl}_2\text{N}_6\text{O}_5\text{Zn}]^+$ ,  $[\text{C}_4\text{H}_8\text{Cl}_2\text{N}_6\text{O}_4\text{Zn}]^+$ ,  $[\text{C}_4\text{H}_5\text{Cl}_2\text{N}_5\text{O}_4\text{Zn}]^+$ ,  $[\text{C}_4\text{H}_5\text{N}_5\text{O}_4\text{Zn}]^+$ ,  $[\text{C}_3\text{H}_4\text{N}_4\text{O}_3\text{Zn}]^+$ , and  $[\text{C}_2\text{H}_3\text{N}_3\text{O}_3\text{Zn}]^+$ , respectively. The fragmentation pattern in Scheme S5 is in agreement with the proposed structure of the Zn(II) complex.



**Figure 6.** The antifungal inhibition zones of Ni(II) complex (a), Cu(II) complex (b), and Zn(II) complex (c) against *Aspergillus oryzae*.

### 3.8. Biological Activity: Antibacterial Screening

Data listed in Table 5 and Figure 6 depict the antibacterial and antifungal properties of the azodicarbonamide ligand and its metal complexes. As an insight into the data, the following remarks can be concluded: The azodicarbonamide and its Zn(II) complex show no antimicrobial activity, and the Ni(II) complex gives significant antifungal activity against *Aspergillus oryzae* and *Penicillium* sp. with inhibition zones of 1.3 and 0.3 cm, respectively. However, it has no antibacterial activity. The Cu(II) complex has acceptable antifungal activity against *Aspergillus oryzae* with the inhibition zone of 0.6 cm.

**Table 5.** The inhibition diameter (cm) of azodicarbonamide ligand and its metal complexes.

No.	<i>Aspergillus oryzae</i>	<i>Penicillium sp.</i>	<i>Bacillus subtilis</i>
Dimethyl sulfoxide	–ve	–ve	–ve
Azodicarbonamide	–ve	–ve	–ve
Ni (II) complex	1.3 cm	0.8 cm	–ve
Cu (II) complex	0.6 cm	–ve	–ve
Zn (II) complex	–ve	–ve	–ve

### 3.9. Computational Studies

Theoretical studies have been performed using DMOL<sup>3</sup> in the Materials Studio package [41–44]. DFT semi-core pseudopotential calculations (dspp) were performed with the double numerical basis sets as well as the polarization function (DNP) [45]. The RPBE function is based on the generalized gradient approximation (GGA) as the best correlation function [46,47]. The structures of the ADCA complexes (Schemes 1–12) depict optimized molecular structures in conjunction with the numbering of the atoms for the azodicarbonamide ligand and its metal complexes. As an insight into data listed in Tables 6–9 for the bond length as well as the bond angles of azodicarbonamide compounds, the following can be concluded:

1. The bond lengths of azodicarbonamide moiety show significant change upon complexation. The remarkable changes were observed for the C(4)-N(1), C(3)-N(2), N(1)-N(2), C(4)-O(5), and O(6)-C(3) bond lengths, which are elongated or shortened depending on the coordination with metal ions [48].
2. The bond angles in the Ni-complex are quite near to its octahedral geometry, predicting sp<sup>3</sup>d<sup>2</sup> or d<sup>2</sup>sp<sup>3</sup> hybridization [49]. The Cu-complex shows a distorted Oh geometry. However, the bond angles in the Zn-complex predict the hexagonal environment around the Zn metal ion.
3. The C(4)-O(5) and C(3)-O(6) bond distances of the carbonyl group in azodicarbonamide are slightly elongated due to the formation of a strong M-O bond which makes the C-O bond weaker [50].
4. The bond distances of Ni-O and Cu-O in Ni- and Cu-complexes are shorter than that of Zn-O in the Zn-complex, reflecting the greater strength of the Ni-N and Cu-N bonds. The bond distances of Ni-N and Cu-N in Ni- and Cu-complexes are shorter than that of Zn-N in the Zn-complex, reflecting the greater strength of Ni-N and Cu-N bonds.
5. The data recorded in Table 10 reveals some quantum chemical parameters, including the energies of frontier molecular orbitals (E<sub>HOMO</sub>, E<sub>LUMO</sub>), the energy band gap (E<sub>H</sub>-E<sub>L</sub>), electronegativity (χ), chemical potential (μ), global hardness (η), global softness (S), and global electrophilicity index (ω), that have been computed according to the following equations [51–53].

$$\chi \text{ (electronegativity)} = -\frac{1}{2} (E_{\text{LUMO}} + E_{\text{HOMO}})$$

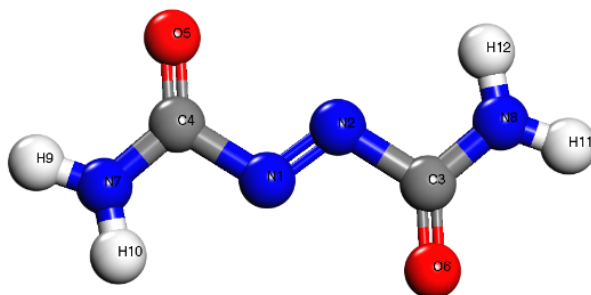
$$\mu \text{ (potential)} = -\chi = \frac{1}{2} (E_{\text{LUMO}} + E_{\text{HOMO}})$$

$$\eta \text{ (hardness)} = \frac{1}{2} (E_{\text{LUMO}} - E_{\text{HOMO}})$$

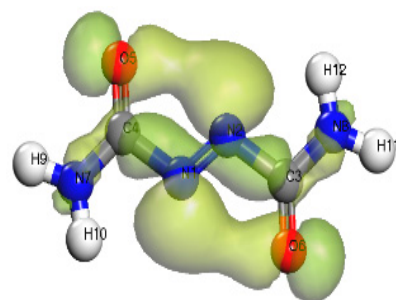
$$S \text{ (softness)} = \frac{1}{2} \eta$$

$$\omega \text{ (electrophilicity)} = \frac{\mu^2}{2\eta}$$

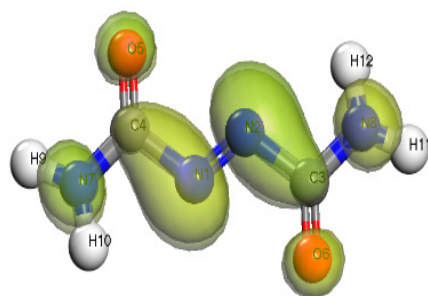
1. The  $\sigma = 1/\eta$  calculated energy band gap for azodicarbonamide is 1.775 eV higher than that of the corresponding metal complexes. In addition, the  $\Delta E_{H-L}$  value for the Ni-complex is the smallest— $\Delta E_{H-L} = 0.957$  eV—which is in a good agreement with the experimental data.
2. The energetic parameters (total energy, binding energy, and dipole moment) have been computed and listed in Table 11. The higher negative values of the binding and total energies for azodicarbonamide complexes indicate the higher stability of the prepared metal compounds compared to that of azodicarbonamide molecule.



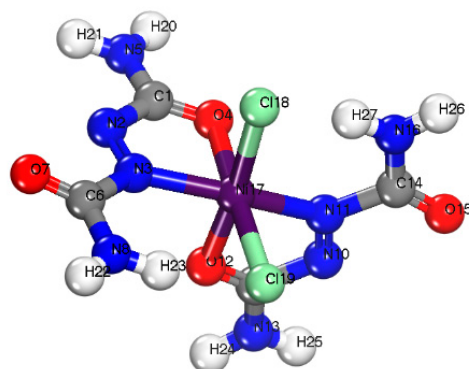
Scheme 1. DFT-optimized geometry of azodicarbonamide ligand.



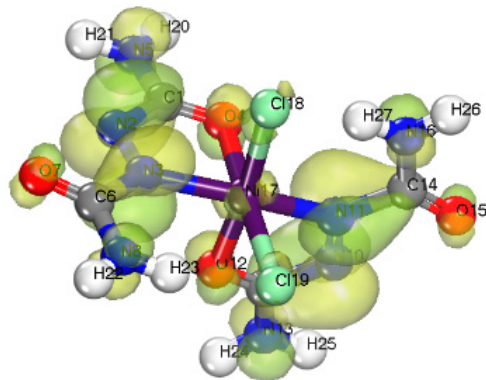
Scheme 2. DFT-optimized geometry of HOMO of azodicarbonamide.



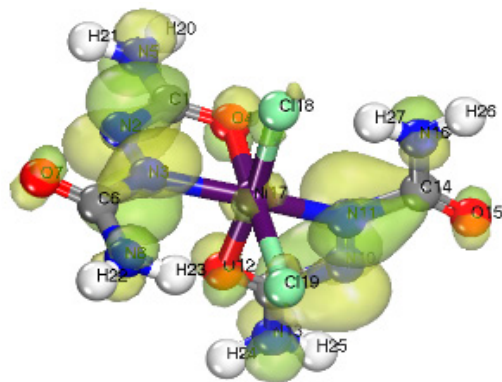
Scheme 3. DFT-optimized geometry of LUMO of azodicarbonamide.



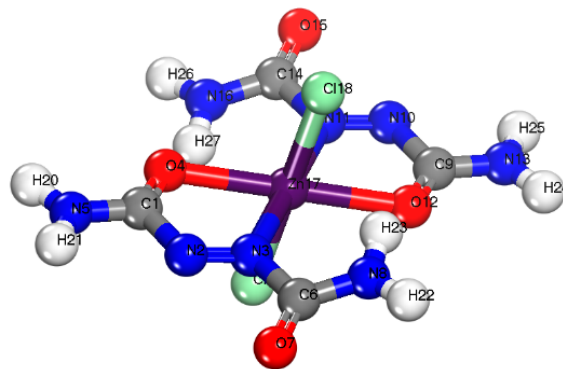
Scheme 4. DFT-optimized geometry of Ni complex.



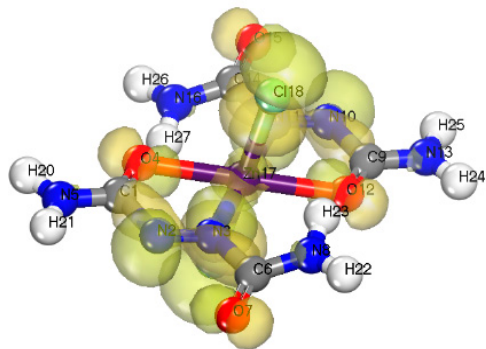
Scheme 5. DFT-optimized geometry of HOMO of Ni complex.



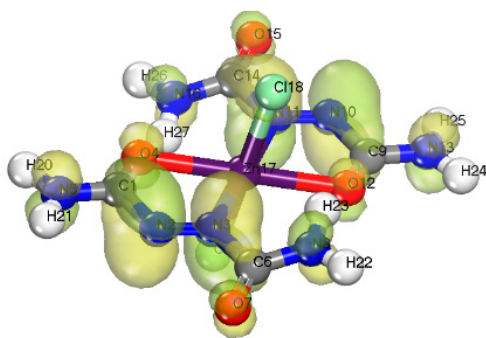
Scheme 6. DFT-optimized geometry of LUMO of Ni complex.



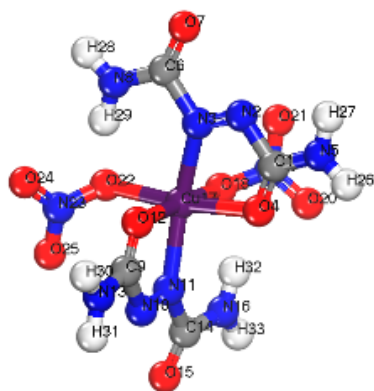
Scheme 7. DFT-optimized geometry of Zn complex.



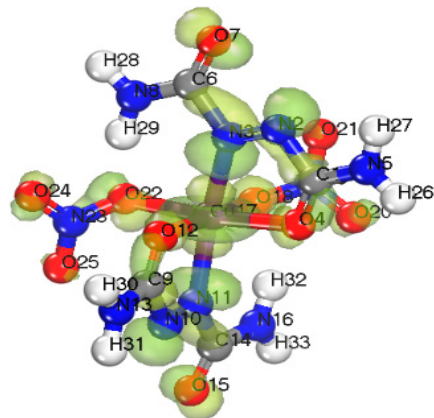
Scheme 8. DFT-optimized geometry of HOMO of Zn-complex.



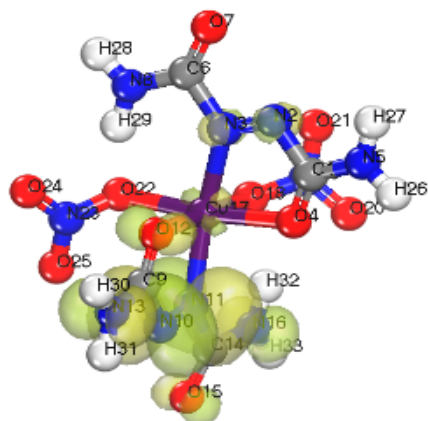
Scheme 9. DFT-optimized geometry of LUMO of Zn-complex.



Scheme 10. DFT-optimized geometry of Cu complex.



Scheme 11. DFT-optimized geometry of HOMO of Cu complex.



Scheme 12. DFT-optimized geometry of LUMO of Cu complex.

**Table 6.** Selected bond lengths (Å) and bond angles (°) of (Ligand) ligand using DFT-method from DMOL<sup>3</sup> calculations.

Bond	Length (Å)	Angle	Degree (°)	Angle	Degree (°)
N(8)-H(12)	1.014	H(12)-N(8)-H(11)	120.799	O(6)-C(3)-N(2)	125.105
N(8)-H(11)	1.015	H(9)-N(7)-C(4)	120.259	C(3)-N(2)-N(1)	111.035
N(7)-H(10)	1.013	N(8)-C(3)-N(2)	107.587	C(4)-N(1)-N(2)	111.047
N(1)-C(4)	1.499	H(12)-N(8)-C(3)	118.942		
N(7)-H(9)	1.014	H(11)-N(8)-C(3)	120.221		
C(4)-N(7)	1.346	H(10)-N(7)-H(9)	120.443		
O(5)-C(4)	1.231	H(10)-N(7)-C(4)	119.245		
N(1)-N(2)	1.248	N(7)-C(4)-O(5)	127.374		
C(3)-N(8)	1.345	N(7)-C(4)-N(1)	107.502		
C(3)-O(6)	1.232	O(5)-C(4)-N(1)	125.113		
N(2)-C(3)	1.499	N(8)-C(3)-O(6)	127.287		

**Table 7.** Selected bond lengths (Å) and bond angles (°) of (Cu complex) ligand using DFT-method from DMOL<sup>3</sup> calculations.

Bond	Length (Å)	Bond	Length (Å)	Angle	Degree (°)	Angle	Degree (°)
N(23)-O(25)	1.253	C(6)-O(7)	1.224	O(22)-Cu(17)-O(18)	86.068	N(11)-Cu(17)-O(4)	92.419
N(23)-O(24)	1.257	C(6)-N(8)	1.336	O(22)-Cu(17)-O(12)	92.414	N(11)-Cu(17)-N(3)	160.538
O(22)-N(23)	1.321	O(4)-Cu(17)	2.206	O(22)-Cu(17)-N(11)	94.457	O(4)-Cu(17)-N(3)	75.274
N(19)-O(21)	1.255	N(3)-Cu(17)	2.161	O(22)-Cu(17)-O(4)	172.959	Cu(17)-O(4)-C(1)	110.239
N(19)-O(20)	1.259	N(2)-N(3)	1.241	O(22)-Cu(17)-N(3)	98.473	Cu(17)-N(3)-C(6)	130.498
O(18)-N(19)	1.317	N(10)-N(11)	1.243	O(18)-Cu(17)-O(12)	176.060	Cu(17)-N(3)-N(2)	117.983
O(22)-Cu(17)	2.189	C(9)-O(12)	1.247	O(18)-Cu(17)-N(11)	101.856	O(12)-Cu(17)-N(11)	74.618
O(18)-Cu(17)	2.186	O(12)-Cu(17)	2.214	O(18)-Cu(17)-O(4)	91.040	O(12)-Cu(17)-O(4)	90.870
C(14)-N(16)	1.338	N(11)-Cu(17)	2.175	O(18)-Cu(17)-N(3)	93.520	O(12)-Cu(17)-N(3)	90.299
C(14)-O(15)	1.223						

**Table 8.** Selected bond lengths (Å) and bond angles (°) of Ni complex ligand using DFT-method from DMOL<sup>3</sup> calculations.

Bond	Length (Å)	Bond	Length (Å)	Angle	Degree (°)	Angle	Degree (°)
Cl(19)-Ni(17)	2.386	N(3)-Ni(17)	2.090	Cl(19)-Ni(17)-Cl(18)	94.535	O(12)-Ni(17)-O(4)	86.609
Cl(18)-Ni(17)	2.386	N(2)-N(3)	1.259	Cl(19)-Ni(17)-O(12)	89.276	O(12)-Ni(17)-N(3)	88.580
C(14)-N(16)	1.340	C(9)-O(12)	1.255	Cl(19)-Ni(17)-N(11)	87.412	N(11)-Ni(17)-O(4)	87.896
C(14)-O(15)	1.229	C(6)-N(8)	1.338	Cl(19)-Ni(17)-O(4)	174.385	N(11)-Ni(17)-N(3)	159.054
O(12)-Ni(17)	2.128	C(6)-O(7)	1.229	Cl(19)-Ni(17)-N(3)	106.982	O(4)-Ni(17)-N(3)	76.757
N(11)-Ni(17)	2.108	O(4)-Ni(17)	2.131	Cl(18)-Ni(17)-O(12)	174.911	O(12)-Ni(17)-O(4)	86.609
N(10)-N(11)	1.259	C(1)-O(4)	1.255	Cl(18)-Ni(17)-N(11)	107.298	O(12)-Ni(17)-N(3)	88.580
				Cl(18)-Ni(17)-O(4)	89.804	Ni(17)-O(12)-C(9)	111.061
				Cl(18)-Ni(17)-N(3)	87.083	Ni(17)-N(11)-C(14)	130.322
				O(12)-Ni(17)-N(11)	76.200	Ni(17)-N(11)-N(10)	118.004
				Ni(17)-O(4)-C(1)	110.225	Ni(17)-N(3)-C(6)	130.593
				Ni(17)-N(3)-N(2)	117.939		

**Table 9.** Selected bond lengths (Å) and bond angles (°) of (Zn complex) ligand using DFT-method from DMOL<sup>3</sup> calculations.

Bond	Length (Å)	Bond	Length (Å)	Angle	Degree (°)	Angle	Degree (°)
Cl(19)-Zn(17)	2.330	C(9)-O(12)	1.244	Cl(19)-Zn(17)-Cl(18)	179.876	Cl(18)-Zn(17)-O(4)	92.703
Cl(18)-Zn(17)	2.328	C(6)-N(8)	1.348	Cl(19)-Zn(17)-O(12)	92.787	Cl(18)-Zn(17)-N(3)	89.164
C(14)-N(16)	1.348	C(6)-O(7)	1.227	Cl(19)-Zn(17)-N(11)	88.952	O(12)-Zn(17)-N(11)	69.365
C(14)-O(15)	1.227	O(4)-Zn(17)	2.309	Cl(19)-Zn(17)-O(4)	87.195	O(12)-Zn(17)-O(4)	179.937
O(12)-Zn(17)	2.310	N(3)-Zn(17)	2.368	Cl(19)-Zn(17)-N(3)	90.867	O(12)-Zn(17)-N(3)	110.695
N(11)-Zn(17)	2.367	N(2)-N(3)	1.246	Cl(18)-Zn(17)-O(12)	87.315	N(11)-Zn(17)-O(4)	110.574
N(10)-N(11)	1.246	C(1)-O(4)	1.244	Cl(18)-Zn(17)-N(11)	91.017	N(11)-Zn(17)-N(3)	179.812
				Zn(17)-O(12)-C(9)	114.409	O(4)-Zn(17)-N(3)	69.366
				Zn(17)-N(11)-C(14)	127.748	Zn(17)-N(11)-N(10)	119.568
				Zn(17)-O(4)-C(1)	114.448	Zn(17)-N(3)-C(6)	127.774
				Zn(17)-N(3)-N(2)	119.543		

**Table 10.** Some quantum chemical parameters of azodicarbonamide and its complexes.

Compound	-E <sub>H</sub>	-E <sub>L</sub>	-E <sub>H-L</sub>	χ	μ	η	S	ω	ϕ
Ligand	5.381	3.606	1.775	4.493	-4.493	0.443	0.2219	22.7510	2.2535
Cu	5.918	4.748	1.170	5.333	-5.333	0.292	0.1462	48.6169	3.4188
Zn	5.787	4.351	1.436	5.069	-5.069	0.359	0.1795	35.7866	2.7855
Ni	5.474	4.523	0.951	4.998	-4.998	0.2377	0.1189	52.5447	4.2061

**Table 11.** Various theoretical molecular parameters of azodicarbonamide and its complexes.

	Dipole Magnitude (D)	Binding Energy (ev)	Total Energy (ev)
Azodicarbonamide	0.1140	-53.5028	-12197.595
Cu-complex	15.1645	-141.43307	-45715.839
Ni-complex	13.1330	-117.59501	-54711.175
Zn-complex	0.0270	-113.57451	-56368.463

#### 4. Conclusions

Physical-chemical studies of novel azodicarbonamide complexes obtained from refluxing the ligand with alcoholic Ni(II), Cu(II), and Zn(II) salt solutions were presented. Elemental, IR, molar conductance, magnetic, UV-vis, mass, and thermal analyses were carried out to confirm the molecular structures of the studied compounds. The vibrational spectra indicate the neutral bidentate behavior of the ADCA ligand. The studied ligand coordinates to metal ions through the oxygen of (C=O)<sub>amidic</sub> and the nitrogen of (N=N)<sub>azo</sub> groups. The molar conductivity measurements prove the non-electrolytic nature of all compounds with 1:2 stoichiometry. Magnetic measurements and electronic spectra predict the paramagnetic and octahedral geometry of copper and nickel complexes, but zinc complex is diamagnetic and has a hexa-coordinated geometry. The energy band gap between HOMO and LUMO for the studied metal complexes is lower than that of the synthesized ADCA ligand, indicating the facility of electron transfer. Ni(II) and Cu(II) complexes can be used as fungicide. However, azodicarbonamide and its zinc complex have no biological efficacy.

**Supplementary Materials:** The following supporting information can be downloaded at: <https://www.mdpi.com/article/10.3390/cryst13030367/s1>, Figure S1: a. FTIR spectrum of pure azodicarbonamide.

b. FTIR spectrum of Ni(II) complex. c. FTIR spectrum of Cu(II) complex. d. FTIR spectrum of Zn(II) complex, Figure S2: a. Mass spectra of Azodicarbonamide ligand [40]. b. Mass spectra of Ni(II) complex. c. Mass spectra of Cu(II) complex. d. Mass spectra of Zn(II) complex, Scheme S1: Decomposition reaction for azodicarbonamide, Scheme S2: Fragmentation pattern of azodicarbonamide ligand, Scheme S3: Fragmentation pattern of Ni(II) complex, Scheme S4: Fragmentation pattern of Cu(II) complex, Scheme S5: Fragmentation pattern of Zn(II) complex.

**Author Contributions:** Conceptualization, A.A.O.Y., A.M.A.A., M.S.R., A.S.A.-W., A.A.A., M.A.A.-O., A.M.N., A.M.A.-O., H.M.A., A.J.O., M.Y.E.-S. and K.A.A.; methodology, A.A.O.Y., A.M.A.A., M.S.R., A.S.A.-W., A.A.A., M.A.A.-O., A.M.N., A.M.A.-O., H.M.A., A.J.O., M.Y.E.-S. and K.A.A.; software, A.A.O.Y., A.M.A.A., M.S.R., A.S.A.-W., A.A.A., M.A.A.-O., A.M.N., A.M.A.-O., H.M.A., A.J.O., M.Y.E.-S. and K.A.A.; validation, A.A.O.Y., A.M.A.A., M.S.R., A.S.A.-W., A.A.A., M.A.A.-O., A.M.N., A.M.A.-O., H.M.A., A.J.O., M.Y.E.-S. and K.A.A.; formal analysis, A.A.O.Y., A.M.A.A., M.S.R., A.S.A.-W., A.A.A., M.A.A.-O., A.M.N., A.M.A.-O., H.M.A., A.J.O., M.Y.E.-S. and K.A.A.; investigation, A.A.O.Y., A.M.A.A., M.S.R., A.S.A.-W., A.A.A., M.A.A.-O., A.M.N., A.M.A.-O., H.M.A., A.J.O., M.Y.E.-S. and K.A.A.; resources, A.A.O.Y., A.M.A.A., M.S.R., A.S.A.-W., A.A.A., M.A.A.-O., A.M.N., A.M.A.-O., H.M.A., A.J.O., M.Y.E.-S. and K.A.A.; data curation, A.A.O.Y., A.M.A.A., M.S.R., A.S.A.-W., A.A.A., M.A.A.-O., A.M.N., A.M.A.-O., H.M.A., A.J.O., M.Y.E.-S. and K.A.A.; writing—original draft preparation, A.A.O.Y., A.M.A.A., M.S.R., A.S.A.-W., A.A.A., M.A.A.-O., A.M.N., A.M.A.-O., H.M.A., A.J.O., M.Y.E.-S. and K.A.A.; writing—review and editing, A.A.O.Y., A.M.A.A., M.S.R., A.S.A.-W., A.A.A., M.A.A.-O., A.M.N., A.M.A.-O., H.M.A., A.J.O., M.Y.E.-S. and K.A.A.; visualization, A.A.O.Y., A.M.A.A., M.S.R., A.S.A.-W., A.A.A., M.A.A.-O., A.M.N., A.M.A.-O., H.M.A., A.J.O., M.Y.E.-S. and K.A.A.; supervision, A.A.O.Y., A.M.A.A., M.S.R., A.S.A.-W., A.A.A., M.A.A.-O., A.M.N., A.M.A.-O., H.M.A., A.J.O., M.Y.E.-S. and K.A.A.; project administration, A.A.O.Y., A.M.A.A., M.S.R., A.S.A.-W., A.A.A., M.A.A.-O., A.M.N., A.M.A.-O., H.M.A., A.J.O., M.Y.E.-S. and K.A.A.; funding acquisition, A.A.O.Y., A.M.A.A., M.S.R., A.S.A.-W., A.A.A., M.A.A.-O., A.M.N., A.M.A.-O., H.M.A., A.J.O., M.Y.E.-S. and K.A.A. All authors have read and agreed to the published version of the manuscript.

**Funding:** This research was funded by the Deanship of Scientific Research at King Saud University through Vice Deanship of Scientific Research Chairs, and the Deanship of Scientific Research at Princess Nourah bint Abdulrahman University through Researchers Supporting Project number (PNURSP2023R35).

**Data Availability Statement:** Data available on the web of journal.

**Acknowledgments:** The authors extend their appreciation to the Deanship of Scientific Research, King Saud University, for the funding through the Vice Deanship of Scientific Research Chairs; (Drug Exploration and Development Chair). The authors are grateful to Princess Nourah Bint Abdulrahman University, Riyadh, Saudi Arabia, for funding this work through Researchers Supporting Project number (PNURSP2023R35).

**Conflicts of Interest:** The authors declare no conflict of interest.

## References

1. Xu, C.; Sun, C.; Wan, H.; Tan, H.; Zhao, J.; Zhang, Y. Microstructure and physical properties of poly(lactic acid)/polycaprolactone/ rice straw lightweight bio-composite foams for wall insulation. *Constr. Build. Mater.* **2022**, *354*, 129216. [[CrossRef](#)]
2. Lei, W.; Wang, D.; Li, Y.; Li, K.; Liu, Q.; Wang, P.; Feng, W.; Liu, Q.; Yang, X. High temperature resistant polymer foam based on bi-functional benzoxazine-phthalonitrile resin. *Polym. Degrad. Stab.* **2022**, *201*, 110003. [[CrossRef](#)]
3. Liu, B.; Essawy, H.; Deng, S.; Zhao, C.; Du, G.; Hou, D.; Zhou, X.; Zhang, J. High performance bio-based gelatinized starch-furanic resin derived foam reinforced by microcrystalline cellulose. *Ind. Crop. Prod.* **2022**, *194*, 116282. [[CrossRef](#)]
4. Douibi, L.; Gouisse, M.; Guessoum, D. Benachour. Synergic Effect of a combined use of two Chemical Blowing Agents on the Foaming Efficiency of an Extruded Rigid PVC Compound. *Int. J. Eng. Technol. Sci.* **2014**, *14*, 60.
5. Sims, G.L.A.; Jaafar, H.A.S. A Chemical Blowing Agent System (CBAS) Based on Azodicarbonamide. *J. Cell. Plast.* **1994**, *30*, 175–188. [[CrossRef](#)]
6. Krutko, I.; Danylo, I.; Kaulin, V. Kinetics of Azodicarbonamide decomposition in the presence of an initiator for obtaining solid foams. *Vopr. Khimii Khimicheskoi Tekhnologii* **2019**, *1*, 26–34.
7. Bryden, J.H. The crystal structure of azodicarbonamide. *Acta Crystallogr.* **1961**, *14*, 61–63. [[CrossRef](#)]
8. Bohloulbandi, E.; Aval, P.A. Study on Catalytic Synthesis of Azodicarbonamide with Hydrogen Peroxide as a Green Oxidant. *Int. J. New Chem.* **2021**, *8*, 356–364.



9. Williams, M.; McEwan, W.; Henry, A.R. the heats of combustion of substituted triazoles, tetrazoles and related high nitrogen compounds. *J. Phys. Chem.* **1957**, *61*, 261–267. [[CrossRef](#)]
10. Beghin, A.S.; Ooms, N.; Hooyberghs, K.; Coppens, E.; Pareyt, B.; Brijs, K.; Delcour, J.A. The influence of varying levels of molecular oxygen on the functionality of azodicarbonamide and ascorbic acid during wheat bread making. *Food Res. Int.* **2022**, *161*, 111878. [[CrossRef](#)]
11. Gao, J.; Guo, Y.; Yan, R.; Liang, J.; Yang, D. Mechanism differences between reductive and oxidative dough rheology improvers in the formation of 1D and 3D gluten network. *Biomaterials* **2022**, *280*, 121275. [[CrossRef](#)] [[PubMed](#)]
12. Rahman, M.M.; Ohm, J.-B.; Simsek, S. Clean-label breadmaking: Size exclusion HPLC analysis of proteins in dough supplemented with additives vs hard red spring wheat flour. *J. Cereal Sci.* **2022**, *104*, 103426. [[CrossRef](#)]
13. Ali Saki, A.-M.T. Influence of Rigid Polyvinylchloride Composites Composition on the Kinetics of Foaming by Azodicarbonamide. Ph.D. Thesis, Moscow State University of Fine Chemical Technologies, Moscow, Russia, 2016. (In Russian).
14. Vasin, A.Y.; Makarov, G.V.; Marinina, L.K.; Yakusheva, Z.A. Kinetics of thermal decomposition of azo compounds. *Izv. Vuzov SSSR Khimiya Khimicheskaya Tekhnologiya* **1980**, *23*, 1070–1074.
15. Gmyzina, R.N.; Mishina, I.M.; Pugacheva, L.A. *Blowing Agents for PVC Foams*; Niiekhim Publishers: Moscow, Russia, 1984; p. 42. (In Russian)
16. Barry, A.L. *The Antimicrobial Susceptibility Test, Principles and Practices*; Lea & Febiger: Philadelphia, PA, USA, 1976; p. 180.
17. Bauer, A.W.; Kirby, W.M.M.; Sherris, J.C.; Turk, M. Antibiotic susceptibility testing by a standardized single disk method. *Am. J. Clin. Pathol.* **1966**, *45*, 493–496. [[CrossRef](#)]
18. Xie, Y.; Li, P.; Zhang, J.; Wang, H.; Qian, H.; Yao, W. Comparative studies by IR, Raman, and surface-enhanced Raman spectroscopy of azodicarbonamide, biurea and semicarbazide hydrochloride. *Spectrochim. Acta Part A Mol. Biomol. Spectrosc.* **2013**, *114*, 80–84. [[CrossRef](#)]
19. Nesterenko, A.M.; Savitskas, V.I.; Polumbrik, O.M.; Markovskii, L.N. Quantum-chemical study of electronic structure and enthalpy of decomposition of azodicarbonamide. *Theor. Exp. Chem.* **1983**, *18*, 480–484. [[CrossRef](#)]
20. Lee, C.; Park, S.-K.; Min, K.-C.; Kim, Y.-S.; Lee, N.-S. Vibrational Analysis and Intermolecular Hydrogen Bonding of Azodicarbonamide in the Pentamer Cluster. *Bull. Korean Chem. Soc.* **2008**, *29*, 1951–1959.
21. Chen, Z.; Wu, Y.; Gu, D.; Gan, F. Spectroscopic, and thermal studies of some new binuclear transition metal(II) complexes with hydrazone ligands containing acetoacetanilide and isoxazole. *J. Spectrochim. Acta Part A* **2007**, *68*, 918–926. [[CrossRef](#)]
22. Padole-Gaikwad, G.S.; Bagade, R.D.; Chaudhary, R.G.; Gharpure, M.P.; Juneja, H. Construction of five new coordination polymers based on maloyl-5-bis-2-aminobenzothiazole: Synthesis, structural, thermal and non-isothermal kinetics. *J. Chin. Adv. Mater. Soc.* **2017**, *5*, 118–132. [[CrossRef](#)]
23. Bhatti, A.S.; Dollimore, D. The effects of additives on the thermal decomposition of azodicarbonamide. *Thermochim. Acta* **1984**, *76*, 273–286. [[CrossRef](#)]
24. Quinn, S. Chemical blowing agents: Providing production, economic and physical improvements to a wide range of polymers. *Plast. Addit. Compd.* **2001**, *3*, 16–21. [[CrossRef](#)]
25. Reyes-Labarta, J.A.; Marcilla, A. Kinetic study of the decompositions involved in the thermal degradation of commercial azodicarbonamide. *J. Appl. Polym. Sci.* **2007**, *107*, 339–346. [[CrossRef](#)]
26. Levai, G.; Nyitrai, Z.S.; Meszlenyi, G. The kinetics and mechanism of the thermal decomposition of azodicarbonamide in polyethylene. II. The effect of zinc oxide. *ACH Model. Chem.* **1999**, *136*, 245–264.
27. Bhatti, A.S.; Dollimore, D.; Goddard, R.J.; O'Donnell, G. The thermal decomposition of azodicarbonamide. *Thermochim. Acta* **1984**, *76*, 63–77. [[CrossRef](#)]
28. Reyes-Labarta, A.; Marcilla, A. Thermal Treatment and Degradation of Cross-Linked Ethylene Vinyl Acetate-Polyethylene-Azodicarbonamide-ZnO Foams. Complete Kinetic Modeling and Analysis. *Ind. Eng. Chem. Res.* **2012**, *51*, 9515–9530. [[CrossRef](#)]
29. Asgari, A.; Ghani, K.; Keshavarz, M.H. Investigating the effect of copper(II) coordination compound with azodicarbonamide ligand on the phase-stabilization of ammonium nitrate. *J. Inorg. Gen. Chem.* **2018**, *17*, 410. [[CrossRef](#)]
30. Fierro, C.M.; Smith, P.D.; Horton, P.N.; Hursthouse, M.B.; Light, M.E. Synthesis and structures of mono and binuclear nickel(II) thiolate complexes of a dicompartmental pseudo-macrocycle with N(imine)<sub>2</sub>S<sub>2</sub> and N(oxime)<sub>2</sub>S<sub>2</sub> metal-binding sites. *Inorg. Chim. Acta* **2011**, *368*, 257–262. [[CrossRef](#)]
31. Lever, A.B.P. *Inorganic Electronic Spectroscopy*; Elsevier: Amsterdam, The Netherlands, 1984.
32. Rashad, M.M.; Hassan, A.M.; Nassar, A.M.; Ibrahim, N.M.; Mourtada, A. A new nano-structured Ni(II) Schiff base complex: Synthesis, characterization, optical band gaps, and biological activity. *Appl. Phys. A* **2013**, *117*, 877. [[CrossRef](#)]
33. Tauc, J. Optical properties and electronic structure of amorphous Ge and Si. *J. Mater. Res. Bull.* **1968**, *3*, 37–46. [[CrossRef](#)]
34. Karipcin, F.; Dede, B.; Caglar, Y.; Hur, D.; Ilican, S.; Caglar, M.; Sahin, Y. A New Dioxime Ligand and Its Trinuclear Copper (II) Complex: Synthesis, Characterisation and Optical Properties. *Opt. Commun.* **2007**, *272*, 131–137. [[CrossRef](#)]
35. Turan, N.; Gündüz, B.; Körkoca, H.; Adigüzel, R.; Çolak, N.; Buldurun, K. Study of Structure and Spectral Characteristics of the Zinc(II) and Copper(II) Complexes with 5,5-Dimethyl-2-(2-(3-nitrophenyl) hydrazono) cyclohexane-1,3-dione and Their Effects on Optical Properties and the Developing of the Energy Band Gap and Investigation of Antibacterial Activity. *J. Mex. Chem. Soc.* **2014**, *58*, 65–75.
36. Sengupta, S.K.; Pandey, O.P.; Srivastava, B.K.; Sharma, V. Trends in Structural Mechanics: Theory, Practice. *Transit. Met. Chem.* **1998**, *23*, 349. [[CrossRef](#)]

37. Fu, M.-L.; Guo, G.-C.; Liu, X.; Liu, B.; Cai, L.-Z.; Huang, J.-S. Syntheses, structures and properties of three selenoarsenates templated by transition metal complexes. *Inorg. Chem. Commun.* **2005**, *8*, 18–21. [[CrossRef](#)]
38. Sisman, I.; Basoglu, A. Effect of Se content on the structural, morphological and optical properties of Bi<sub>2</sub>Te<sub>3</sub>–ySe<sub>y</sub> thin films electrodeposited by under potential deposition technique. *Mater. Sci. Semicond. Process.* **2016**, *54*, 57. [[CrossRef](#)]
39. Urbach, F. The Long-Wavelength Edge of Photographic Sensitivity and of the Electronic Absorption of Solids. *Phys. Rev.* **1953**, *92*, 1324. [[CrossRef](#)]
40. Stadler, R.H.; Mottier, P.; Guy, P.; Gremaud, E.; Varga, N.; Lallji, S.; Whitaker, R.; Kintscher, J.; Dudler, V.; Read, W.A.; et al. Semicarbazide is a minor thermal decomposition product of bazodicarbonamide used in the gaskets of certain food jars. *Analyst* **2004**, *129*, 276–281. [[CrossRef](#)]
41. Pettit, L.; University of Leeds, Leeds, UK. Personal Communication, 1993.
42. Delley, B. A Scattering Theoretic Approach to Scalar Relativistic Corrections on Bonding. *Int. J. Quantum Chem.* **1998**, *69*, 423–433. [[CrossRef](#)]
43. Delley, B. From molecules to solids with the DMol3 approach. *J. Chem. Phys.* **2000**, *113*, 7756–7764. [[CrossRef](#)]
44. Kessi, A.; Delley, B. Density functional crystal vs. cluster models as applied to zeolites. *Int. J. Quantum Chem.* **1998**, *68*, 135–144. [[CrossRef](#)]
45. *Materials Studio*; Version 2020; Accelrys Software Inc.: San Diego, CA, USA, 2019.
46. Hehre, W.J.; Radom, L.; Schlyer, P.V.R.; Pople, J.A. *AB Initio Molecular Orbital Theory*; Wiley: New York, NY, USA, 1986; ISBN 978-0-471-81241-8.
47. Hammer, B.; Hansen, L.B.; Nørskov, J.K. Improved adsorption energetics within density-functional theory using revised Perdew-Burke-Ernzerhof functionals. *Phys. Rev. B* **1999**, *59*, 7413–7421. [[CrossRef](#)]
48. West, D.X.; Swearingen, J.K.; Valdes-Martinez, J.; Hernandez-Ortega, S.; El-Sawaf, A.K.; van Meurs, F.; Castineiras, A.; Garcia, I.; Bermejo, E. Spectral and structural studies of iron(III), cobalt(II,III) and nickel(II) complexes of 2-pyridineformamide N(4)-methylthiosemicarbazone. *Polyhedron* **1999**, *18*, 2919–2929. [[CrossRef](#)]
49. Despaigne, A.A.R.; Da Silva, J.G.; Do Carmo, A.C.M.; Piro, O.E.; Castellano, E.E.; Beraldo, H. Copper (II) and zinc (II) complexes with 2-benzoylpyridine-methyl hydrazone. *J. Mol. Struct.* **2009**, *920*, 97–102. [[CrossRef](#)]
50. Hocking, R.K.; Hambley, T.W. Structural Measure of Metal-Ligand Covalency from the Bonding in Carboxylate Ligands. *Inorg. Chem.* **2003**, *42*, 2833–2835. [[CrossRef](#)] [[PubMed](#)]
51. El-Sherif, A.A.; Fetoh, A.; Abdulhamed, Y.K.; Abu El-Reash, G.M. Synthesis, structural characterization, DFT studies and biological activity of Cu(II) and Ni(II) complexes of novel hydrazine. *Inorg. Chim. Acta* **2018**, *480*, 1–15. [[CrossRef](#)]
52. Abu El-Reash, G.A.; El-Gammal, O.A.; Radwan, A.H. Molecular structure and biological studies on Cr (III), Mn (II) and Fe (III) complexes of heterocyclic carbohydrazone ligand. *Spectrochim. Acta Mol. Biomol. Spectrosc.* **2014**, *121*, 259–267. [[CrossRef](#)] [[PubMed](#)]
53. Yousef, T.A.; Abu El-Reash, G.M.; El Morshedy, R.M. Quantum chemical calculations, experimental investigations and DNA studies on (E)-2-((3-hydroxynaphthalen-2-yl)methylene)-N-(pyridin-2-yl)hydrazinecarbothioamide and its Mn(II), Ni(II), Cu(II), Zn(II) and Cd(II) complexes. *Polyhedron* **2012**, *45*, 71–85. [[CrossRef](#)]

**Disclaimer/Publisher’s Note:** The statements, opinions and data contained in all publications are solely those of the individual author(s) and contributor(s) and not of MDPI and/or the editor(s). MDPI and/or the editor(s) disclaim responsibility for any injury to people or property resulting from any ideas, methods, instructions or products referred to in the content.